UC San Diego

UC San Diego Previously Published Works

Title

New methods for measuring atmospheric heavy noble gas isotope and elemental ratios in ice core samples

Permalink

https://escholarship.org/uc/item/31q692q2

Journal

Rapid Communications in Mass Spectrometry, 32(10)

ISSN

0951-4198

Authors

Bereiter, Bernhard
Kawamura, Kenji
Severinghaus, Jeffrey P

Publication Date

2018-05-30

DOI

10.1002/rcm.8099

Peer reviewed

eScholarship.org Powered by the California Digital Library
University of California

Received: 13 October 2017 | Revised: 21 February 2018 | Accepted: 22 February 2018

DOI: 10.1002/rcm.8099

RESEARCH ARTICLE

WILEY Rapid Communications in Mass Spectrometry

New methods for measuring atmospheric heavy noble gas isotope and elemental ratios in ice core samples

Bernhard Bereiter[1,2,3] | Kenji Kawamura[4,5,6] | Jeffrey P. Severinghaus[1]

[1] Scripps Institution of Oceanography, University of California San Diego, La Jolla, CA 92037, USA

[2] Climate and Environmental Physics, Physics Institute, and Oeschger Center for Climate Research, University of Bern, 3012 Bern, Switzerland

[3] Laboratory for Air Pollution/Environmental Technology, Empa, 8600 Dübendorf, Switzerland

[4] National Institute of Polar Research, Research Organizations of Information and Systems, 10-3 Midori-cho, Tachikawa, Tokyo 190-8518, Japan

[5] Department of Polar Science, Graduate University for Advanced Studies (SOKENDAI), 10-3 Midori-cho, Tachikawa, Tokyo 190-8518, Japan

[6] Institute of Biogeosciences, Japan Agency for Marine-Earth Science and Technology, 2-15 Natsushima-cho, Yokosuka 237-0061, Japan

Correspondence
B. Bereiter, Laboratory for Air Pollution/ Environmental Technology, Empa, Überlandstrasse 129, 8600 Dübendorf, Switzerland.
Email: bereiter@climate.unibe.ch

Funding information
Japan Society for the Promotion of Science, Grant/Award Number: 21671001, 26241011, 15KK0027, 17H06320; National Science Foundation, Grant/Award Number: 05-3863009-44343; Schweizerischer Nationalfonds zur Förderung der Wissenschaftlichen Forschung, Grant/Award Number: P2BEP2_152071

Rationale: The global ocean constitutes the largest heat buffer in the global climate system, but little is known about its past changes. The isotopic and elemental ratios of heavy noble gases (krypton and xenon), together with argon and nitrogen in trapped air from ice cores, can be used to reconstruct past mean ocean temperatures (MOTs). Here we introduce two successively developed methods to measure these parameters with a sufficient precision to provide new constraints on past changes in MOT.

Methods: The air from an 800-g ice sample – containing roughly 80 mL STP air – is extracted and processed to be analyzed on two independent dual-inlet isotope ratio mass spectrometers. The primary isotope ratios ($\delta^{15}N$, $\delta^{40}Ar$ and $\delta^{86}Kr$ values) are obtained with precisions in the range of 1 per meg (0.001‰) per mass unit. The three elemental ratio values $\delta Kr/N_2$, $\delta Xe/N_2$ and $\delta Xe/Kr$ are obtained using sequential (non-simultaneous) peak-jumping, reaching precisions in the range of 0.1–0.3‰.

Results: The latest version of the method achieves a 30% to 50% better precision on the elemental ratios and a twofold better sample throughput than the previous one. The method development uncovered an unexpected source of artefactual gas fractionation in a closed system that is caused by adiabatic cooling and warming of gases (termed adiabatic fractionation) – a potential source of measurement artifacts in other methods.

Conclusions: The precisions of the three elemental ratios $\delta Kr/N_2$, $\delta Xe/N_2$ and $\delta Xe/Kr$ – which all contain the same MOT information – suggest smaller uncertainties for reconstructed MOTs (±0.3–0.1°C) than previous studies have attained. Due to different sensitivities of the noble gases to changes in MOT, $\delta Xe/N_2$ provides the best constraints on the MOT under the given precisions followed by $\delta Xe/Kr$, and $\delta Kr/N_2$; however, using all of them helps to detect methodological artifacts and issues with ice quality.

1 | INTRODUCTION

Global ocean temperatures play a fundamental role in the Earth's climate system, but existing constraints on past changes and natural variability are weak. This is mainly due to the heterogeneity of ocean temperatures, which makes it difficult to retrieve a globally integrated signal. In a pioneering work, Headly and Severinghaus[1] showed the feasibility of reconstructing past atmospheric krypton (Kr) to nitrogen ratios ($\delta Kr/N_2$) based on ice core measurements, and the potential of this parameter to be a truly integrative proxy of global mean ocean temperatures (MOTs). The precision of $\delta Kr/N_2$ reached in that study, however, was not enough to improve the existing constraints on MOTs given mainly by ocean sediment proxies (i.e. Elderfield et al[2]). The primary goal of the method used in Headly and Severinghaus[1] was to

 Copyright © 2018 John Wiley & Sons, Ltd.

test the basic concept of the proxy and the feasibility of reconstructing heavy noble gas mixing ratios from ice core samples. Here we present two advanced methods (denoted Method 1 and Method 2) that aim for high precision of these parameters while we also add Kr isotope ratios to the suite of analytes. With these methodological advances the potential of past noble gas mixing ratios from ice cores as a proxy for MOT can be further exploited.

The atmosphere contains only traces of heavy noble gases, with 1.1 ppm of Kr and 0.087 ppm of Xe. Even the relatively large variations in ocean temperature associated with glacial–interglacial cycles affect these concentrations only in the per mil range.[1,3] Therefore, to achieve adequate precision a certain sample volume is required; however, sample air from ice cores is limited by the nature of the archive (ice core samples are precious and they only contain around 100 cm^3 STP of air per kg of ice). The explorative method of Headly and Severinghaus[1] used a sample size of only 50 g of ice (resulting in about 4cm^3 STP sample air in their case) which was enough to measure Kr with adequate precision, but not enough for the less abundant Xe. Therefore, the follow-up methods described here were developed to process about 800 g ice samples (providing about 80 cm^3 STP sample air), which enable measurement of the $\delta Xe/N_2$ ratio with adequate precision and also provide enough sample to measure Kr isotope ratios. While the $\delta Xe/N_2$ ratio can serve as a MOT proxy in a similar way to $\delta Kr/N_2$,[1] Kr isotopes do not change in the atmosphere and so provide additional constraints on the air fractionation processes in the firn column[4] that need to be taken into account for correcting the raw ice core sample data.[1]

With the first generation of the follow-up methods (Method 1, see also Headly[5]) the main goals of obtaining $\delta Xe/N_2$ and Kr isotopes with adequate precision were achieved. However, the main weakness of this method is the need for overnight equilibration of the sample in a water bath, which limits the sample throughput to one sample per day, with a minimum of three days from the start of the sampling to obtain results. Combined with the very delicate mass spectrometry needed for a measurement campaign, as well as the complex labor required for this method, it is not a suitable method for larger campaigns. We therefore developed a second method, Method 2, with the aim of speeding up the sample throughput and also simplifying the labor involved, while at the same time improving the precision compared with Method 1. The primary innovation of Method 2 is a low-pressure equilibration chamber that takes advantage of the faster molecular diffusion at low pressure, to speed up the equilibration and splitting step (4 h instead of overnight).

The main objective of this work is to describe the two new methods. A first version of Method 1 is also found in the dissertation of Headly.[5] To avoid future referencing of non-peer-reviewed literature, we describe Method 1 in full detail here, while we also include the most recent adaptations to this method and an extensive performance test that is not part of Headly.[5] The work here focuses on the technical aspects and the best practices (to our knowledge) to reach the highest precision to date in this type of measurement. At the end we assess the constraint on MOT based on the new improved precision gained with the new methods. In addition, we show that good quality ice and its identification form the basis for reliable paleoatmospheric data. For further application of the data derived here for MOT reconstructions and other scientific goals, the reader is referred to Headly and Severinghaus,[1] Ritz et al,[3] Kawamura et al,[4] Headly,[5] Buizert and Severinghaus,[6] and Bereiter et al.[7]

2 | EXPERIMENTAL

2.1 | Sample processing

The basic principle of the methods to measure heavy noble gas elemental ratios in ice samples is shown in Figure 1. The details of each part of the method are explained in the following subsections. Here we give a short summary. In a first step, the air trapped in the ice sample is extracted by melting the ice under vacuum. Roughly 80 mL STP of sample air is required for this analysis, corresponding to roughly 800 g of ice. In a second step, the extracted air is split into two subsamples: a whole air sample and a noble gas sample. The latter is obtained by gettering all the non-noble gases on a Zr/Al getter material. The reason for the split is that the precision of the noble gas measurements is greatly improved by the gettering; but the δKr/Ar and δXe/Ar ratios are not well preserved in ice core samples due to

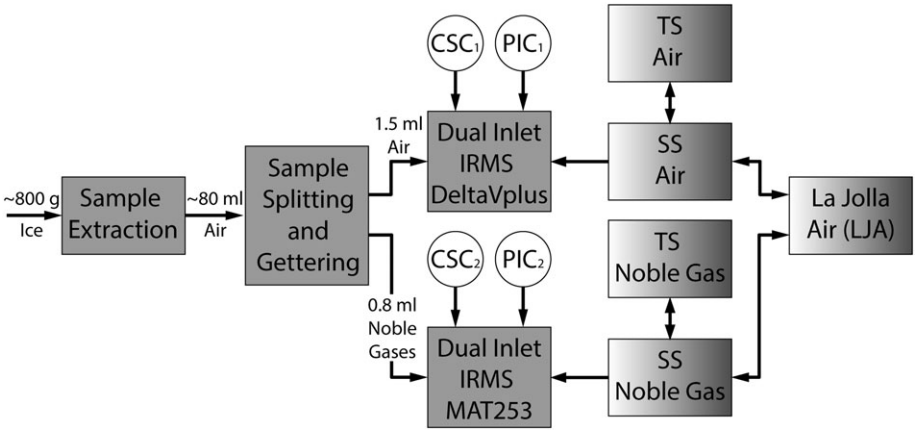

FIGURE 1 Overview of sample processing and analysis. Sample processing goes from left to right. CSC = chemical slope correction; PIC = pressure imbalance correction; TS = tertiary standard; SS = secondary standard. See section 2.1 for details about the first two steps and section 2.4 for the other elements of the process

leakage of Ar out of the bubbles.[8] Therefore, the $\delta Ar/N_2$ ratio is also needed for post-measurement computation of the $\delta Kr/N_2$ and $\delta Xe/N_2$ ratios, which are well preserved.[9]

The two subsamples are measured on separate dual-inlet isotope ratio mass spectrometers, both of which have secondary (SS) and tertiary working standards (TS) containing a gas that has been adjusted to approximately match the samples (whole air and noble gases). The SS is used as the reference gas for each subsample measurement. The TS is occasionally compared with the SS to track possible mass spectrometer instabilities, changes in zero enrichments, and/or drifts of the SS. The SSs are referenced to our absolute primary standard, which is modern atmospheric air. This primary standard – which we call La Jolla Air (LJA) – is air sampled via a non-fractionating method at the Scripps Pier in La Jolla (CA, USA).[10] All the results given here are expressed as a difference of ratios relative to LJA (δ-notation) following Coplen:[11]

$$\delta(x) = \frac{R^x_{\text{sample}}}{R^x_{\text{LJA}}} - 1, \quad (1)$$

where R^x denotes the number ratio of elements x obtained in the sample and LJA, respectively. Note that δ-values are usually small numbers and are therefore given in per mil (‰, 10^{-3}), or in our case mostly in per meg (10^{-6}).

The sample processing comprises the sample extraction, sample splitting and sample gettering part. In Method 1, the extraction and gettering parts are combined on one processing line (see Figure 2) and the splitting in the isothermal water bath is done in an external line attached to the main line when needed. In Method 2, the main line of Method 1 is only used for sample extraction and a second vacuum line is used for splitting and gettering (Figure 2). This allows parallel sample processing with Method 2 and, hence, speeds up the sample throughput.

2.2 | Extraction (common to both methods)

The extraction of the air from the ice follows closely the prior protocols of Kawamura et al,[4] Headly,[5] and Severinghaus and Battle.[9] In a −25°C freezer room, an ice sample with roughly 800 g weight is prepared. The effective sample size varies from core to core because of the different air content, which varies primarily due to the elevation of the ice deposition site.[12] For samples with high air content as from the WAIS Divide ice core (110 mL STP/kg), about 700 g are enough. For samples with low air content such as from the Taylor Glacier (90 mL STP/kg), about 900 g are needed. The maximum sample size that was processed with the current method is around 1.2 kg of ice. This is limited by the melting vessel dimensions.

Cracks in the ice are avoided as much as possible or cut out of the sample, and a minimum of about 2 mm of ice is shaved from each surface of the sample ice to limit potential contamination caused by gas diffusion through the ice lattice.[13] The sample is placed in a stainless steel melting vessel of roughly 2.5 L in volume together with a glass encapsulated stir bar and sealed with a ConFlat® flange. The sample is then transported to the laboratory in a box and placed in a freezer to avoid warming of the vessel.

In the laboratory, the vessel is attached to the extraction line using an Ultra-Torr® connection and kept cool with an ethanol bath at −20°C. The vessel is then evacuated through water trap 1 using the vacuum pumps (a turbo-molecular pump and an oil-free roughing pump in series). Water trap 1 is a double trap cooled with liquid nitrogen to protect the pumps from water vapor and to keep the vacuum lines dry.

Once the majority of the air in the melting vessel has been pumped out, we evacuate the freshly attached vacuum lines, the melting vessel surfaces, and the ice sample surfaces via sublimation for 20 min. A leak check is performed during this phase to make sure that the new connections and the melting vessel are leak tight (criterion for passing a leak check is that the pressure on P1 does not rise more than 1–4 Torr in 30 s when the pump is closed off).

After this pump-down period, the valves are switched such that the evacuation passes through water trap 2 instead of water trap 1 (closing V3, V4 and V5; opening V2, V6 and V7). Water trap 2 is a glass bead trap, which in Method 1 was cooled with an ethanol bath at roughly −80°C.[5] It was difficult to control the ethanol bath temperature, so we replaced it with an automated PID-regulated liquid nitrogen nozzle for Method 2. This device is able to stabilize the trap temperature at −100 ± 1°C (note that Xe starts to be trapped below −110°C). The nozzle introduces liquid nitrogen into a Dewar in which a small fan mixes the cold nitrogen gas.

After the switch to water trap 2, the cryo-trapping of the sample air at 4 K is started (closing V10, opening V9) and the ethanol bath (at the melting vessel) is removed and replaced with a warm water bath at roughly 40°C such that the water just touches the bottom of the vessel. This marks the start of the effective extraction phase which takes about 60 min.

During the first 20–30 min of this phase the ice is melted, and the air extraction rate must be controlled to not exceed a level that would cause water vapor to break through water trap 2. From experience the break-through can occur when P1 (capacitive pressure gauge) reads above 2 Torr, so the pressure is kept below this level by manually controlling the water bath temperature and its level. We keep the water temperature above 30°C by adding hot water as needed, and slowly raise the water level from the bottom of the vessel to the top, while constantly stirring the water bath and measuring its temperature. At the beginning, the melting is slow because a water layer has not yet formed between the ice and the vessel floor, which conducts heat to the ice. Once the layer has formed, melting is rapid. To minimize surface degassing from the inner walls of the vessel, the water bath level is kept below the inner water level so as to only warm the water in which the ice is sitting. Because we cannot observe the inner water level, some experience is required for this process.

After 20–30 min the pressure reading on P1 shows a quick drop below the 0.1 Torr level. This marks the end of the melting phase and the point in time that the water bath is removed. Again, some experience is needed to recognize the end of the melting and it is important not to wait too long as this could cause warming of the water and a clogging of the water trap, due to the strong vapor pressure dependence on temperature. Now the glass-encapsulated magnetic stir bar inside the vessel is actuated to help degas the melt water. This degassing phase comprises the rest of the 60-min extraction phase, which is critical for the complete extraction of xenon. During this phase the dip tube is lowered into the liquid helium in about two steps to expose fresh stainless steel surface area in order to keep the cryo-trapping efficient for the remaining gases.

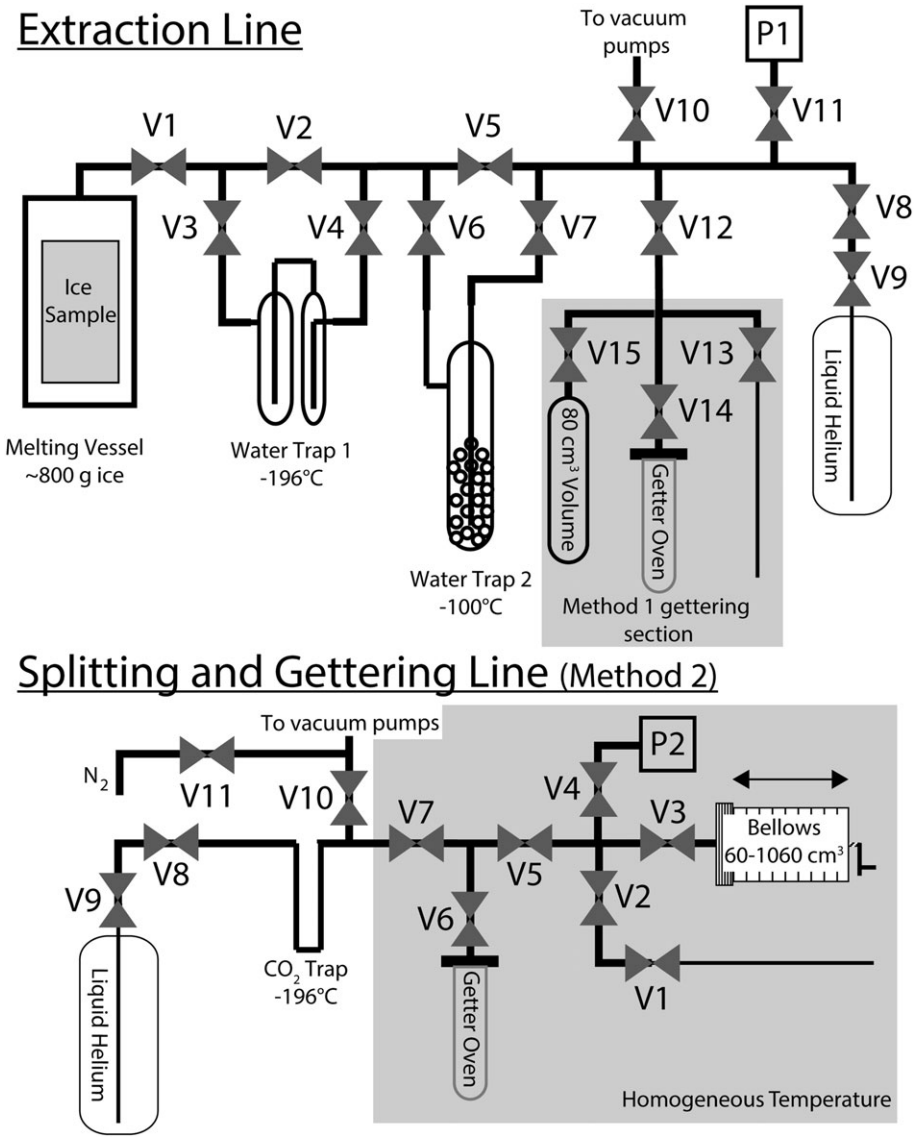

FIGURE 2 Sample processing lines used in the two methods described here. Top: Extraction line used in both methods to extract the trapped air from the ice sample and collect the air in the dip tube to the right via cryo-trapping. This is the main working line for Method 1 for which the getter section (gray square) is attached to V12. In Method 2 this part is not used. All tubing including the dip tube is made of stainless steel with the exception of the traps and getter, which are made of glass. The outer diameter (OD) size is 1/2" for the main lines, 3/8" around the traps, and 1/4" for the dip tube. Bottom: The splitting and gettering line is used only for Method 2. The collected air from the extraction line, contained in a dip tube, is attached to V2 for introduction. All tubing is also made of stainless steel (except for the CO_2 trap and getter, which are glass) and uses VCR® connections. Between the bellows, V1, trap and the vacuum pumps the tubing size is 1/2" OD. The dip tubes and the section around V8 are 1/4" OD, while the trap is 3/8" OD. The temperature-homogenized section (gray square) is in a plywood box in which a small air fan circulates the air. The tubing in this section is not directly mounted to the metallic hanger assembly but only touches wood, in order to isolate the tubing from the lab temperature. With this approach the temperature in the box is homogenized usually within 0.05°C as observed with two temperature sensors attached to the tubing at distant spots in the box

Towards the end, a stable pressure of a few millibar should be reached at P1, which is due to the helium in the ice sample that cannot be cryo-trapped. Now the sample dip tube is closed (V9) and removed from the liquid helium tank.

2.3 | Splitting and gettering (Method 1)

The dip tube with the sample air is attached to two leak-tight stainless steel expansion volumes of 180 cm^3 and 4 cm^3, respectively.[5] To ensure a minimal leak rate, only VCR® connections are used in this assembly. The 4 cm^3 volume can be separated from the rest with a valve. The sample air is expanded into the expansion volumes and the whole assembly is submerged in a water bath. The water bath ensures a highly homogenized temperature field within the assembly, which otherwise would degrade the measurement due to thermal fractionation of the gases. The assembly is left in the isothermal bath for at least 12 h to homogenize the gases within the assembly. Afterwards, the valve between the two expansion volumes is closed while still in the water bath, completing the non-fractionating split of the sample air.

The two subsamples are now transferred into separate dip tubes via cryo-trapping at 4 K, as in section 2.1. Here our standard transfer procedure consisting of 10 min of cryo-trapping in total is applied.[8,14]

For the transfer of the whole air subsample (in the 4 cm^3 volume), a CO_2 trap consisting of a 3/8" OD Pyrex U-trap at 77 K is interposed (equal to trap in Figure 2, bottom). After this step, processing of the whole air subsample is finished and the corresponding dip tube is placed in the queue for analysis (see section 2.4).

The dip tube containing the large volume subsample (from the 180 cm^3 volume) is attached to the extraction line (V13 in Figure 2, top) for gettering. The getter oven (a ½" OD quartz glass tube wrapped with heating wire) is filled with 36 Zr/Al getter sheets and connected to the vacuum pumps. In an initial 10-min cleaning and activation phase, the getter oven is heated to 100°C, followed by a second such phase for which the oven is heated to 900°C. After this, the pumps are closed off (closing V12) and the sample air is expanded into the 900°C hot getter oven and the 80 cm^3 volume (opening V13 and V15). The 80 cm^3 volume is needed to pull the bulk of the sample air out of the dip tube and bring it into proximity to the getter for efficient gettering. The 900°C Zr/Al now starts to absorb all gases except the noble gases.

After 10 min, the sample dip tube is closed (V13) while gettering is continued for another 10 min. The oven temperature is then lowered to 300°C to let the getter absorb H_2 for the next 5 min before it is switched off. The first portion of the gettered sample is then transferred into a fresh dip tube using the standard transfer procedure, except that the dip tube is not removed from the liquid helium after closing the dip tube valve. The gettering is now repeated for the portion of the sample left in the dip tube, for 20 min at 900°C followed by 5 min at 300°C. This portion is then transferred into the same dip tube as the first one. This technique reduces the background pressure of Ar in the second gettering step to ensure fast molecular diffusion and complete removal of N_2. After this step processing of the second subsample (noble gas sample) is finished and the dip tube is placed in the queue for analysis (see section 2.4).

2.4 | Splitting and gettering (Method 2)

Method 2 employs a large (1060 cm^3) stainless steel bellows to permit the creation of temporary low gas pressures which increase the diffusive homogenization and, hence, speed up the splitting process. The bellows also permit efficient gettering and cryo-trapping after the split is complete, by compressing the bellows to reduce the system volume. The required isothermal state during the splitting is achieved by an air temperature homogenizing system instead of the water bath. The sample processing for this new method proceeds as follows.

The dip tube with the sample air is attached to the new splitting and gettering line at V1 (Figure 2, bottom). First, the sample air is expanded into the fully extended bellows (V4, V5 closed; V1, V2, V3 open). Our standard routine consists of one cycle of pumping with the bellows, which means that V2 is closed, the bellows compressed to its minimum, V2 opened and closed again and the bellows extended again to its maximum, and V2 opened again. The idea of this pumping sequence is to reduce the initial gas fractionation inherited from the dip tube by mixing via induced turbulence (the gases in the dip tube are highly fractionated due to cryo-trapping). We carry out only one of these sequences because more such sequences were found to increase the fractionation (see section 3.2).

Now, the temperature insulation box (see Figure 2) is closed and the air mixing fan in that box turned on. Depending on whether the sample air has been extracted on the same day or on the day before, we leave the system in this configuration for a minimum of 6 and 4 h, respectively. This time is needed to homogenize the sample air completely in the system by molecular diffusion (see section 3.1 for more details). After the equilibration time is over the temperature difference between two distant spots in the box is recorded (usually below 0.05°C) and the sample is split (closing V1).

Now the getter oven is prepared and cleaned/activated in the same way as in Method 1 (see section 2.2). The gettering is then started (closing V7; opening V5) and the bellows is compressed to its minimum. In contrast to Method 1, no two-step gettering is needed here, due to improved gas diffusion arising from the shorter path length for the gases to diffuse to the getter material, and the larger-diameter tubing leading to the getter oven. All non-noble gases are removed in a single run of 55 min of gettering at 900°C followed by 5 min at 300°C (to absorb H_2). Now this noble gas subsample is transferred into a new dip tube, which will be put in the queue for IRMS analysis (see section 2.5). Afterwards, the whole air subsample remaining in the line is also transferred into a new dip tube for analysis through the same type of CO_2 trap as in Method 1.

2.5 | Mass spectrometry

The mass spectrometry protocol builds on the work of Headly and Severinghaus,[1] Headly,[5] Severinghaus et al,[8] and Orsi.[10] The noble gas subsample is analyzed on a MAT 253 isotope ratio mass spectrometer (Thermo Fisher Scientific, Bremen, Germany) that contains 8 Faraday cups/measurement channels. The whole air sample is analyzed on a Delta-V Plus isotope ratio mass spectrometer (Thermo Fisher Scientific) that contains 6 Faraday cups/measurement channels. Both spectrometers are specifically configured for the needs of the method described here (see Table 1 for details). These dedicated spectrometers provide better ion current statistics and more measurement channels/parameters than Headly and Severinghaus[1] had available, providing better control over potential artifacts. Following the previous work, we also apply a "pressure imbalance correction" (PIC) and "chemical slope correction" (CSC) on both machines. The PIC factor is subject to changes on weekly timescales and is calibrated at least once a week during a measurement campaign. The CSC factor is more stable/smaller and is usually calibrated once per measurement campaign.

For both mass spectrometers the sample tubes are connected to the corresponding instrument using VCR® connections (sample side), while the secondary standards (SSs) are attached to the standard sides. The SSs (and TSs) are contained in a 2-L stainless steel welded cylindrical can with a small pipette volume (1.3 cm^3) at the exit for removal of an unfractionated aliquot. The same gas inlet procedure is undertaken on both machines. First, the evacuated pipette volume is closed towards the spectrometer and opened towards the SS and equilibrated with the SS for 10 min. During this time both bellows of the dual-inlet system (40 cm^3) are cleaned from the previous sample and expanded eventually to their maximum. After the 10 min, the SS pipette volume is separated from the main volume, and both the

TABLE 1 Characteristics of measurement sequences run on the two dual-inlet isotope ratio mass spectrometers

Measurement sequence	Air	Argon	Krypton	Ar-Kr	Ar-Xe
Mass spectrometer model	Delta-V Plus	MAT 253	MAT 253	MAT 253	MAT 253
Observed masses	28/29/32/34/40/44	36/38/40	82/83/84/86	40/84	40/132 (129)
Faraday cups	1/2/3/4/5/6	1/2/6	3/4/5/7	6/5	6/6 (4)
Amplification resistors [Ω]	3e8/3e10/1e9/ 3e11/1e10/1e12	1e11/1e12/3e8	1e12 for all	3e8/1e12	3e8/1e12(1e12)
PB mass/Beam intensity [V]	28/4	36/5.5	84/4.0	36/5.5	36/5.5
Integration time [s]	8	8	16	8/16	8/16
Idle time [s]	8	8	16	8/16	8/16
Changeover cycles	16	16	25	6	12
Block repetitions	4–8	3–4	4	3	2

The content of lines two to four (masses, cups and resistors) follows the same order from left to right and characterizes each measurement channel of the instrument in the corresponding measurement mode. The fifth line describes the parameters that are used for the pressure balancing (PB), which is done at the beginning of each block. One block is defined as a set of changeover cycles (sample-standard change over) following a single pressure balancing and peak centering step. On the MAT 253 the methods are run in sequence from left to right of the table. The final result of a sample is given by the mean of the pressure-corrected and chemical slope-corrected block means and its uncertainty by the standard deviation of that mean, taking into account the low number of blocks with an inverse t-function.

sample and the SS aliquot are then expanded into the corresponding bellows. The gases are then equilibrated with the bellows for another 10 min, after which the bellows are closed to the inlets and the corresponding measurement sequences are started. In the early stages of Method 1 the two equilibration phases were only 3 min long[5]; it was subsequently found that the precision could be improved using a 10-min equilibration.

The Delta-V Plus mass spectrometer allows the simultaneous collection of six ion beams between masses 28 and 44, thus producing $\delta^{15}N$, $\delta^{18}O$, $\delta O_2/N_2$, $\delta Ar/N_2$ and $\delta CO_2/N_2$ values simultaneously (see details in Table 1). The main target ratios of this measurement are the $\delta^{15}N$ and $\delta Ar/N_2$ values. The $\delta CO_2/N_2$ values are only used for quality control (due to the isobaric interference caused to the $\delta^{15}N$ value of CO^+ produced in the mass spectrometer ion source from CO_2 that might have escaped removal and/or leaked into the sample). Depending on whether we target $\delta^{18}O$ values, a more extensive pretreatment of the dip tubes with pure O_2 to passivate the metal surfaces may be carried out before a measurement campaign. This is due to oxidation processes in the dip tubes that can raise $\delta^{18}O$ values and reduce $\delta O_2/N_2$ values.

On the MAT 253 mass spectrometer several different measurement sequences are run in series (see Table 1) to obtain $\delta^{40}Ar$, $\delta^{86}Kr$, δKr/Ar and δXe/Ar values. The latter two are measured using a "peak-jumping" method in which the spectrometer magnet setting is changed sequentially between argon and krypton, or argon and xenon (we amended the peak-jumping method to collect ^{40}Ar instead of ^{36}Ar as was done in Headly[5]). One changeover cycle in these peak-jumping methods contains a standard and sample comparison in the first magnet setting followed by a similar comparison in the second magnet setting. We run 6 (12) cycles for δKr/Ar (δXe/Ar) ratios, calculate a δ-value for each cycle, and use the average over these δ-values as our reported value. In another amendment to the Ar-Xe peak-jumping method, ^{129}Xe was collected simultaneously with ^{132}Xe in the xenon magnet setting to get a rough estimate of the $\delta^{132}Xe$ value. As expected, this ratio shows much larger uncertainty than the other isotope ratios due to the inherently low precision of the peak-jumping method.

For most parameters from Method 2 (Flasks 1–9, Table 2), the overall machine error (obtained by measuring the two working standards SS and TS against each other) is very similar to the total method error (including artifacts introduced by the sample processing). This shows that for these parameters Method 2 reaches the limit given by the mass spectrometer and it is not limited by the sample

TABLE 2 Top section: Comparison of the total method precisions for Methods 1 and 2 (Flasks 1–9, see also Figure 4). The primary target parameters are underlined. The secondary parameters are mainly for quality control purposes (see also section 5). The data show standard deviations in per meg units (0.001‰) of a total of n repeated LJA samples taken from m different flasks. The ratios $\delta Kr/N_2$ and $\delta Xe/N_2$ are derived by combining $\delta Ar/N_2$ measured by the Delta-V Plus with the δKr/Ar and δXe/Ar ratios obtained by the MAT 253 mass spectrometer. Bottom section: Corresponding uncertainties in reconstructed Mean Ocean Temperatures (MOTs) based on the analytical uncertainties of the $\delta Kr/N_2$, $\delta Xe/N_2$ and δXe/Kr values using the box model as described in section 4

Parameter	Mass ratio	Method 1	Method 2 Flasks 1–6	Method 2 Flasks 7–9
m	-	4	6	3
n	-	11–13	27–28	9–14
$\underline{\delta^{15}N}$	29/28	3.3	2.2	0.7
$\delta^{18}O$	34/32	7	16	7
$\underline{\delta^{40}Ar}$	40/36	4	6/7 (14)	3
$\delta^{40}Ar(38)$	40/38	7	8	8
$\underline{\delta^{86}Kr}$	86/82	16	15	15
$\delta^{86}Kr(84)$	86/84	12	13	23
$\delta^{86}Kr(83)$	86/83	25	25	26
$\underline{\delta^{132}Xe}$	132/129	-	-	140
$\delta O_2/N_2$	32/28	140	680	200
$\delta Ar/N_2$	40/28	105	24	17
$\underline{\delta Kr/N_2}$	84/28	200	150	130
$\underline{\delta Xe/N_2}$	132/28	310	240	130
δXe/Kr	132/84	210	180	110
MOT [°C]	$\delta Kr/N_2$ $\delta Xe/N_2$ δXe/Kr	0.32 0.18 0.2	0.24 0.14 0.17	0.21 0.08 0.1

processing (extraction and splitting/gettering) as for Method 1. The exceptions are the $\delta^{18}O$ and $\delta O_2/N_2$ values (machine precisions of 4 per meg and 16 per meg, respectively), which are altered due to the oxidation effects in the dip tubes. These effects, however, can be controlled by pretreatment of the dip tubes. In summary, the most recent changes included in Method 2 have significantly improved the precision. To further enhance the precision of these types of measurements the mass spectrometric analysis would need to be improved.

3 | TESTS AND EVALUATION

As mentioned above, the main goal of Method 2 was to increase the sample throughput. The limiting factor in Method 1 is the equilibration time (T_E) of a minimum of 12 h (see section 2.2). By introducing the large volume bellows into the system (see Figure 2, bottom) we reduced the pressure during the equilibration roughly by a factor of 5, which in principle reduces the equilibration time by a factor of 5. However, T_E is also dependent on other factors such as the geometry of the system or the fractionation condition in the dip tube at the beginning. Therefore, we measured T_E for the new system under realistic conditions that apply to our routine procedure.

3.1 | Sample equilibration and splitting

The target of the experiments described here was to derive the minimum equilibration time T_E required in the new system. To test this we cryo-trapped about 80 mL STP of dry LJA in a dip tube. The tube was attached to V2 at the new splitting line (Figure 2) followed by the equilibration procedure described in section 2.3, with the negligible difference that the air was expanded with V5 open, but V6 and V7 closed (the added volume to the standard equilibration procedure is about 2%). After a certain time, we closed V1 and V5 and analyzed the air trapped in the volume V5-V6-V7 and in the dip tube on the Delta-V Plus. The difference between the two sections of the system is used as a measure of the progress of the equilibration (see Figure 3). We carried out these experiments for samples that were

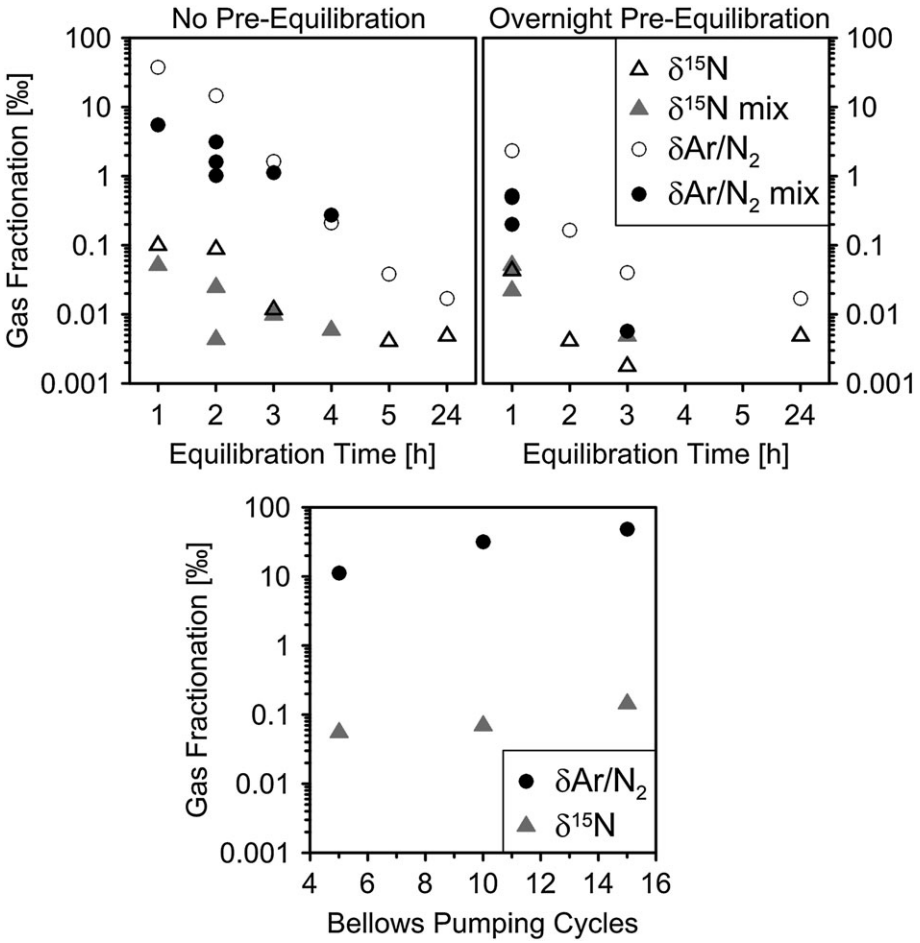

FIGURE 3 Top panels: Dependence of gas fractionation in the new splitting line (Figure 2) on different equilibration times. The data show standard deviations of the results from the two volumes (see text). The dip tube volume shows in all cases initially negative values in $\delta^{15}N$ and positive values in $\delta Ar/N_2$ compared with the other volume (note that the plotted standard deviation is positive by definition). Open symbols: no mixing cycles (see section 2.3) applied prior to equilibration. Solid symbols: 3 mixing cycles applied prior to equilibration. Left: sample is equilibrated shortly after cryo-trapping. Right: sample is equilibrated the day after cryo-trapping. Bottom panel: Gas fractionation in the new splitting line relative to the number of pumping cycles with the bellows. The anomalous values in $\delta^{15}N$ and in $\delta Ar/N_2$ of the tube volume compared with the other volume become larger with the number of pumping cycles. The data were obtained after 30 min of equilibration. The bellows pumping procedure is described in section 2.3

cryo-trapped just before the experiments (no pre-equilibration), and for samples that were cryo-trapped on the day before (overnight pre-equilibration).

The results displayed in the top panels of Figure 3 show an exponentially (log y-axis) decreasing difference in the $\delta^{15}N$ and $\delta Ar/N_2$ values between the two sampled volumes. This is expected from a purely molecular diffusion-driven equilibration process following the release of a highly inhomogeneous gas mixture. Due to the cryo-trapping in the dip tube, gases apparently become highly fractionated owing to their different sublimation temperatures. Since the sublimation temperatures of different elements (here N_2 and Ar) are very different from between isotopologues of the same element, the initial fractionation of $\delta Ar/N_2$ value is much stronger (1–2 orders of magnitude) than that of the $\delta^{15}N$ value.

The initial positive $\delta Ar/N_2$ values and negative $\delta^{15}N$ values in the tube relative to the other volume is not straightforward to understand (note, that Figure 3 show standard deviations, which are positive by definition). We explain this by two different effects related to the thawing of the gases in the tube after it is removed from the liquid helium tank. For the $\delta Ar/N_2$ value, Ar sublimates after N_2 due to its higher sublimation temperature. Although Ar is probably frozen higher up in the tube and closer to the inlet of the tube due to the higher freezing temperature, N_2 sublimates before Ar and passes the still-frozen Ar, filling up the area near the tube outlet/valve. In this way a concentrated N_2 plume fills up the volume near the tube outlet and will leave the tube first when it is expanded into the system, leaving Ar-enriched air behind in the dip tube. For $\delta^{15}N$ values ($^{29}N_2/^{28}N_2$), we speculate that the effect is a consequence of the faster diffusivity in air of the lighter isotopologue than the heavier one. During the cryo-trapping process, the gases have to diffuse towards the cold dip tube which leads to an enrichment of the heavier isotopologues in the gas frozen out last. When the tube is warmed up, the layers frozen out last will thaw first and, hence, the tube will be filled first with gas enriched in the heavy isotopologue. Because N_2 is frozen out near the dead end of the dip tube which is bathed in the cold liquid helium, the gas enriched in heavy isotopologues becomes concentrated near the tube exit, and follows the same logic as for the $\delta Ar/N_2$ values.

The dip tube will equilibrate slower than the rest of the volume due to the long (1 m), thin (1/4″) geometry of the tube and its low-conductance valve. Therefore, the equilibration of the $\delta Ar/N_2$ value in the tube that we measured in this experiment is a conservative indicator for the total equilibration of the gases in the system. Since Kr and Xe also have higher sublimation temperatures than N_2, the enrichment of these gases in the dip tube is probably comparable. Based on the lower gas diffusivities of these heavier gases, Kr and Xe probably equilibrate slower within the system. However, due to the larger measurement uncertainty associated with these gases and the fact that we actually measure them at the larger portion of the splitting volume, we think that the equilibration time indicated by the $\delta Ar/N_2$ value is also a good estimate for the heavier gases. In any case, we measure LJA through the same procedure and equipment as the unknowns, so any small bias will also occur in LJA air and thus be canceled out when we normalize to LJA.

Without pre-equilibration, a minimum of about 6 h is required to equilibrate the sample in the new system. The comparison between the results using a three-cycle mixing procedure at the beginning of the equilibration (see section 2.3) and the one without mixing (empty vs solid data points in Figure 3, top panels) shows a tendency toward smaller gas fractionation for the mixed ones. We think that this is a real and beneficial effect of the mixing procedure on the equilibration, and three cycles are still below the number at which adiabatic fractionation becomes dominant (see section 3.2). However, for our standard routine described in section 2.3 we adopt a conservative approach and apply only one mixing cycle.

For tubes that have been pre-equilibrated, a minimum of 4 h equilibration time is found to be necessary. This shorter equilibration time allows us to increase the sample throughput to two samples per day. To make this possible, the first sample extracted on a specific day is equilibrated over the following night with enough time to reach the minimum of 6 h while the second sample from the same day can be equilibrated the next day, only needing a minimum of 4 h.

Compared with Method 1, these equilibration timescales are about a factor two longer than expected from first-order approximations (see section 3). The 12 h for Method 1 derived by Headly[5] was based only on the measured $\delta^{15}N$ value, which needs less time to equilibrate than the $\delta Ar/N_2$ value (see Figure 3) and could in fact explain the factor-of-two discrepancy. Headly[5] mentions that the $\delta Ar/N_2$ values still suggested a small disequilibrium after 12 h but regarding the overall method precision at that time, this was not considered as critical. The first-order approximation, however, could also be simplistic and secondary effects related to the geometry and adsorption/desorption effects in the equilibration unit could also play a role. Note that for practical reasons the equilibration in Method 1 is typically done overnight, for which reason the effective equilibration time in this method is usually 18 h or more; however, this might still be a bit too short and a reason why Method 1 shows a slightly worse performance than Method 2.

3.2 | Adiabatic cooling- and warming-induced gas fractionation (adiabatic fractionation)

The reason that the equilibration takes several hours is that concentration gradients within the gas have to be homogenized by the slow molecular diffusion process. If it were possible to "stir" the gas, the equilibration step could go much faster. It is, however, not straightforward to stir gas in a closed vacuum system without contaminating it. During our equilibration tests we considered "stirring" the gas by quickly pumping the gas back and forth in the system via compression of the metal bellows. We reasoned that these fast gas movements would create turbulence at small features in the tubing and, hence, mix the gases.

The results (Figure 3, bottom panel) show that the fractionation between the two sampled volumes increased with number of pumping cycles, contrary to the expectation of induced mixing by turbulences. The pumping cycles that we carried out are characterized by a factor of 10 volume change and a repetition time of around 10–30 s. Considering the relatively long repetition time, we expect a significant temperature buffering with the tubing walls and, hence, the process is

only partly adiabatic. However, in the idealized purely adiabatic case the temperature change is about 450°C. Even if the effective warming is only a fraction of this due to the non-adiabatic share/heat buffering of the walls, this still creates adequate leverage for severe thermal fractionation.[15] We hypothesize that the effect is caused by this adiabatic heating and cooling of the gas in the following way. During the compression, the gas temperature adiabatically increases and becomes higher than that of the surrounding tubing. This drives an enrichment of heavy molecules towards the cold walls of the tubing. During expansion, the gas temperature becomes lower than that of the surrounding walls and the effect reverses, but because the pumping system consists of two sections with very different surface-to-volume ratios and conductance for the gas flow (bellow vs dip tube), the effects do not cancel out.

Interestingly, we observe an opposite thermal signal in the $\delta^{15}N$ and $\delta Ar/N_2$ values (note that the standard deviations shown in Figure 3 are positive by definition), which indicates that other processes are also at work. For example, pressure fractionation which might occur at the bellow-tube transition during the fast compression/expansion could also play a role.[15] In addition, surface adsorption effects in the thin tube might be relevant and could explain why the elemental ratio $\delta Ar/N_2$ behaves differently from the isotope ratio $\delta^{15}N$, because adsorption characteristics usually differ between elements, but not (so much) between isotopologues. It is known, for example, that Ar adsorbs preferentially relative to N_2 in response to gas pressure increases in the stainless steel capillaries of the mass spectrometer.

For a deeper understanding of the relevant processes and their magnitudes a numerical model using the true geometry of the system seems necessary. The large temperature changes and the corresponding thermal fractionation potential during the pumping experiments seem to be the logical driving element for the fractionation that we observe, but the geometry and other processes also seem to play an important role. Despite our incomplete understanding of the fractionation process that we observe here, the adiabatic-like pumping with the bellows, as was done here, increases the fractionation in our system after each cycle (Figure 3). The underlying mechanism is clearly related to the adiabatic warming and cooling in the process and is therefore distinct from "thermal fractionation", which is usually understood as a isobaric process or "kinetic fractionation" and "barometric pumping", which are isothermal processes.[4,6] Due to the strongly undesirable effect of adiabatic fractionation on the homogenization of our sample, we reduced the pumping cycle to one stroke in our standard processing procedure (see section 2.3).

3.3 | La Jolla Air (LJA) reference measurements

As in Headly and Severinghaus,[1] our measurements are referenced to the modern atmosphere using direct atmospheric samples taken from the Scripps Pier in La Jolla (called La Jolla Air (LJA)). The same non-fractionating procedure as described in Headly and Severinghaus[1] to collect LJA is used, with the difference that the series of 4-cm^3 volumes was replaced with one 2-L glass flask.[10] From such a 2-L flask up to five LJA aliquots of 80 cm^3 STP can be taken, as shown by the fact that none of the parameters have a systematic trend over the course of five such aliquots (see Figure 4). This suggests that there is no significant fractionation in the taking of an aliquot.

To capture the impact of small artifacts that may be induced by the method, these LJA samples are processed on the principle of equal treatment to ice samples. For practical reasons we do not, however, mimic the slow ice extraction process and the water vapor transport into the water trap occurring during air extractions from ice samples (some prior experiments by Severinghaus et al[8] used degassed ice with LJA to improve the realism of the procedure; these did not find any significant effects). Our LJA aliquots are transferred within 10 min under dry conditions through the cold water trap 2 (see Figure 2, top) into a dip tube. Any subsequent processing is identical to that of the air from ice samples (see section 2.1).

The results of repeated LJA measurements (Figure 4) represent the long-term stability of Method 2. The parameters derived with the Delta-V Plus (crosses) do not show any significant trends and biases over this long period, demonstrating the long-term stability of these parameters. The results are expressed as the deviation from the SS, as they are derived from the raw data from the mass spectrometers. In particular the SS of the MAT 253 is mixed from commercially obtained pure gases such that it approximately matches the expected mixing ratios from the samples, which are gravitationally enriched in the heavy noble gases. This is why the LJA values are negative relative to the SS for most cases.

For the data obtained with the MAT 253 (triangles), significant shifts for all elemental ratios (δKr/Ar, δXe/Ar, δXe/Kr) and $\delta^{40}Ar$ values are found over the course of the period shown in Figure 4. Note that the δXe/Kr ratios are not independently analyzed on the MAT 253, but rather calculated from the δKr/Ar and δXe/Ar values. However, by comparing the δKr/Ar, δXe/Ar and δXe/Kr values, it is possible to identify which ion beam was responsible for a certain shift. For example, the δKr/Ar and δXe/Ar values are lower for the January 2015 set than for the surrounding sets, which is not the case for the δXe/Kr values. This shows that the shift is probably caused by a change in the Ar beam.

An ice sample measurement campaign is started and ended by a set of LJA samples as shown in Figure 4. In order to reference the ice sample results to the modern atmosphere, LJA reference values for each parameter and point in time are required. In normal cases, the means of the two bracketing sets are used for this reference LJA value, and the standard deviation of these data is taken as the analytical uncertainty for each individual sample (ice samples are too large, and ice too precious, to allow the taking of replicates for uncertainty estimates). In cases where there is a clear indication of a trend or shift in these reference values from the SS vs. TS measurements, which are obtained on a regular basis, a linear interpolation between the two sets is used or each set is used separately up to a certain point in the bracketed campaign.

The latter case applies to the shift in $\delta^{40}Ar$ values between sets in January and April 2015. During the measurement campaign between these sets we had to change the ion source filament in the MAT 253. This clearly caused a corresponding shift in the $\delta^{40}Ar$ values as identified by the surrounding SS vs. TS measurements (not shown here). Therefore, for the sampling campaign between the two LJA sets, the January 2015 set is used as the reference for the $\delta^{40}Ar$ values before the filament change, and the April 2015 set for the

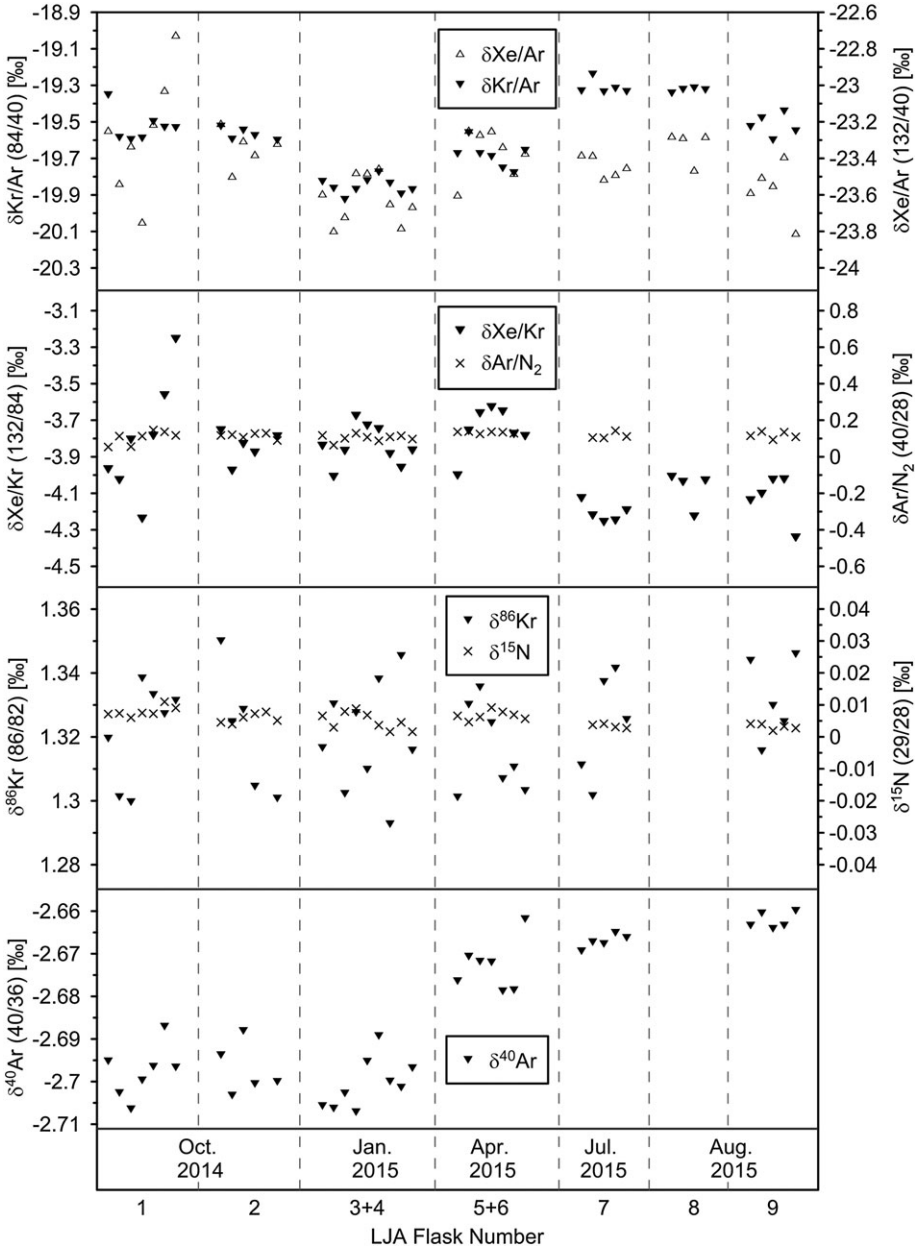

FIGURE 4 Repeated LJA measurements over the course of a year using Method 2. Data show the mean values of the sequences (see Table 1) run on the two mass spectrometers (crosses = Delta-V; triangles = MAT 253) for one LJA sample relative to the SS. Data are organized in sets of consecutive measurements, which are used to determine the LJA reference value for the ice sample measurements in between these sets. Note that the filament had to be replaced between Jan. 2015 and Apr. 2015, which caused the corresponding shift in δ^{40}Ar values

values afterwards. For all other parameters no such separation is done to the LJA reference value. The standard deviations given in Table 2 for the δ^{40}Ar value and Flasks 1–6 show the effect of this LJA value separation on the derived precision. The value in the brackets shows the standard approach if we were to use both sets together. The other two values show what the value would be if we were to accept the filament effect and use the first and second set individually. It clearly shows that the standard approach would lead to larger uncertainties than can be expected from a stable mass spectrometer.

In general, the approach to deal with system instabilities and uncertainties described here provides an objective measure of the analytical performance of the method for the period it has been used. The performance can slightly change over time mainly because the mass spectrometers do not always perform at the same level of stability (as seen in Figure 4). Also, it is important to include all the observed parameters in the assessment of method performance, as not all parameters react equally to a certain disturbance (as seen for example by the effect of filament change on the δ^{40}Ar value in Figure 4). With regard to an objective reconstruction of heavy noble gas ratios in the atmosphere and their application for mean ocean temperature reconstructions, a similar concept is recommended. By using all three noble gas ratios (δKr/N_2, δXe/N_2 and δXe/Kr) for ocean temperature reconstructions, an artifact introduced by a methodological problem is likely to fractionate the three ratios differently, such that the inferred ocean temperatures from the three ratios would diverge from each other. The disagreement of the three proxies thus serves as a quality control flag.

4 | CONSTRAINT ON GLOBAL MEAN OCEAN TEMPERATURES (MOT)

As shown in Headly and Severinghaus[1] and Ritz et al,[3] changes in atmospheric $\delta Kr/N_2$, $\delta Xe/N_2$ and $\delta Xe/Kr$ values can be used as a direct measure of changes in MOT based on the solubility of these gases in ocean water. We use a two-box model consisting of one ocean and one atmosphere box to derive the uncertainty to be expected in the MOT based on the analytical uncertainties that we derived here. Ritz et al.[3] showed that such a simple model is sufficient to describe the link between the MOT and noble gas mixing ratios (unless equilibration with the ocean is not changed, i.e. by sea-ice as modeled in Ritz et al[3]).

To infer MOT changes (relative to today) from a given $\delta Kr/N_2$, $\delta Xe/N_2$ or $\delta Xe/Kr$ value, we use the box model in a forward mode and infer MOT values by iterating the input MOT until the given atmospheric δ value is reached within 1 per meg (0.001 ‰). In detail, the model works as follows: the total amount (moles) of dissolved gas x in the ocean (MO_x) is calculated by:

$$MO_x(T) = sol_x(T,S)\cdot V_O\cdot\rho, \tag{2}$$

where $sol_x(T,S)$ is the equilibrium gas solubility function providing the dissolved amount of the gas x in seawater at 1-atm pressure of air (mol/kg) which depends on the seawater temperature T and salinity S. In the case described here with a single ocean box, T corresponds to MOT and S to the average global ocean salinity (34.72 PSS[16]). The $sol_x(T,S)$ functions are taken from Headly and Severinghaus,[1] which uses the parameters of Hamme and Emerson[17] for N_2 and Xe and of Weiss and Kyser[18] for Kr. V_O is the total ocean volume of 1.335×10^{18} m^3 (ETOPO1) and ρ the average density of seawater of 1027.51 kg/m^3.[16] Note that the $sol_x(T,S)$ functions have been derived for a moist atmospheric air mixture and, hence, already include the partial pressures of the corresponding gases.

Our measurement is by definition relative to the current atmospheric composition. Due to mass conservation of noble gases in the ocean–atmosphere system,[1,3] an observed deviation from the current atmospheric composition corresponds to the change in dissolved moles of gas in the ocean relative to today. For today (t = 0) the dissolved amount is defined by the current MOT (T_0) = 3.53°C.[16] The difference $MO_x(T_0) - MO_x(T_1)$ represents the change in total dissolved moles in the ocean due to the corresponding change in MOT of period t = 0 relative to period t = 1. This change in dissolved moles has to be provided by the atmosphere due to mass conservation in the ocean–atmosphere system. Using the total amount of moles in the atmosphere MA:

$$MA = \frac{V_a}{V_{st}}, \tag{3}$$

with V_a being the total dry atmosphere volume of 3.97e18 m^3[33] and V_{st} the standard volume of one mole of gas (0.02241 m^3/mol), we can calculate the change in molar fraction in the atmosphere of gas x (MA_x) as follows:

$$MA_x(T_t) = \frac{MO_x(T_0) - MO_x(T_t)}{MA} \tag{4}$$

Based on this, the change in atmospheric mixing ratio of gas x_1 relative to x_2 for a given change in MOT (T_t) is calculated as follows (δ-notation, see Equation 1):

$$\delta x_1/x_2(T_t) = \left(\frac{\left(FA^0_{x_1} + MA_{x_1}(T_t)\right)/\left(FA^0_{x_2} + MA_{x_2}(T_t)\right)}{FA^0_{x_1}/FA^0_{x_2}} - 1\right), \tag{5}$$

where FA^0 denotes the molar fraction of gas x in the current atmosphere. The results of this model are basically identical to those obtained with the corresponding box model of Ritz et al.[3] Note that the definition of the solubility function in Ritz et al[3] (denoted as β) is per 1-atm pressure of gas x, and not per 1-atm pressure of air, for which reason the partial pressure appears in their formulae.

We can now derive the expected constraints on MOT based on the measurement uncertainties of the $\delta Kr/N_2$, $\delta Xe/N_2$ and $\delta Xe/Kr$ values given in Table 2. For this a Monte Carlo simulation is performed in which for each parameter 1000 δ-values are generated with a distribution around zero corresponding to the given uncertainties. For each of these values the box model is iteratively run forward to find the MOT that fits the δ-value within 1 per meg (0.001 ‰). The standard deviation of the output MOT for each species is given in Table 2 (bottom) and represents the constraint on MOT as limited by the analytical uncertainties of the $\delta Kr/N_2$, $\delta Xe/N_2$ and $\delta Xe/Kr$ values in the atmospheric samples presented in section 3.3.

This, however, does not necessarily have to be equal to the uncertainty obtained for trapped air in ice samples due to (1) gas fractionation effects during the extraction process which can be difficult to control, and (2) effective variations in the trapped air between neighboring/replicate samples. The second point can occur, e.g., when gas loss after ice core drilling has significantly altered the trapped air.[8] These gas loss effects depend strongly on the storage temperature and duration,[13] for which reason ice that has been drilled not too long ago and which has been stored carefully at low temperatures is preferred. The data shown in Figure 5 (see section 5) were obtained from such well-preserved ice (WAIS Divide). The data from above and below the BCTZ – which cover a period where the MOT is expected to be stable and which therefore can be considered as first-order replicates – show variability consistent with the uncertainty derived from the atmospheric samples. This suggests that the potential additional sources of noise are not substantial. Furthermore, a recent extensive study on ice samples[7] shows that the data variability is consistent with the uncertainty from atmospheric samples throughout the whole record. Nevertheless, as shown in section 5, the quality of the ice and its history since the drilling are essential for a successful retrieval of unaltered atmospheric heavy noble gas ratios from ice core samples.

5 | DETECTING BAD ICE QUALITY: THE BUBBLE TO CLATHRATE TRANSITION ZONE (BCTZ)

In order to reconstruct ocean temperatures following Headly and Severinghaus,[1] the trapped gas must be well preserved in the ice. In any deeper ice core there exists the so called Bubble-to-Clathrate-Transition-Zone (BCTZ) (or Brittle Ice Zone)[19] in which the preservation of trapped gases is problematic due to post-coring fractionation processes (i.e. gas loss)[20] and fractionation between the co-existing

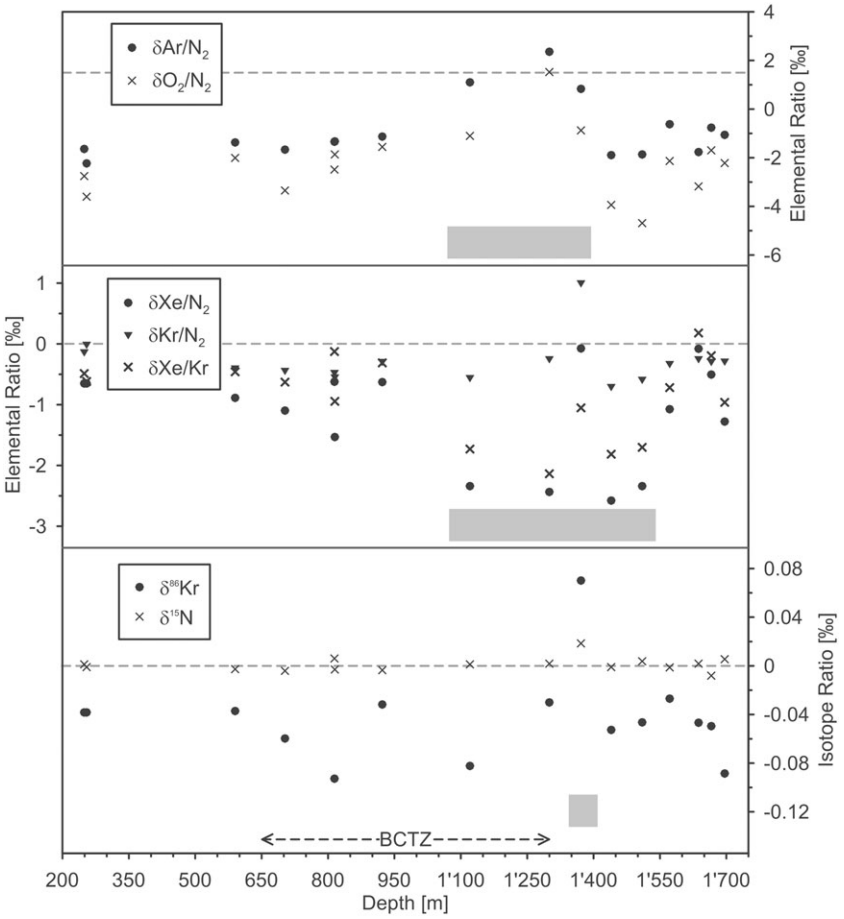

FIGURE 5 Parameters of trapped gases in ice samples from the WAIS Divide ice core (this study and Bereiter et al[7]) obtained with Methods 1 and 2, covering the last roughly 10,000 years (Holocene). All parameters are corrected for gravitational enrichment of the heavy isotopologues in the bottom of the stagnant firn column using measured $\delta^{40}Ar$ values.[1] The data are indicative of the negative effects of the BCTZ by the abnormal patterns seen in the parameters relative to surrounding parameters. The gray bars mark the data which appear altered by the BCTZ, while the dashed arrow shows the BCTZ location derived from visual observation of the ice. Top panel: $\delta Ar/N_2$ and $\delta O_2/N_2$ with the positive excursions in $\delta Ar/N_2$ caused by the BCTZ, as seen in Kobashi et al.[20] Middle panel: Noble gas elemental ratios $\delta Kr/N_2$, $\delta Xe/N_2$ and $\delta Xe/Kr$, showing that the BCTZ causes a spread among different ratios, and suggesting that this effect occurs in a wider depth range than previously recognized. Bottom panel: Isotope ratios, which show clear anomalies for only one data point

gas enclosures.[21] The negative effects of the BCTZ on the solid ice quality (brittleness) and on the trapped gas quality do not necessarily overlap with each other. The effects in the gas records are usually not found in the top half of the BCTZ, but instead are pronounced towards the lower end with a "tailing-off" behavior below the BCTZ.[20-22] Nevertheless, the final alteration in the trapped gases is a complex combination of the different effects and is difficult to quantify/model. Therefore, the best practice in the ice core gas research community to identify the "BCTZ-affected" depth range is currently to measure the target parameters within and around the BCTZ, and put the results into the context of the expected climatic variations over the covered time period. This has not yet been done for the heavy noble gas ratios obtained here.

One sensitive indicator for (BCTZ) alterations in the trapped gases is the $\delta Ar/N_2$ value. After correction for firn fractionation processes, in "good" ice this parameter is slightly negative due to preferential loss of Ar during bubble close-off,[9] but shows strong positive excursions around the BCTZ due to preferential loss of N_2 after coring.[20] We therefore use firn-fractionation-corrected $\delta Ar/N_2$ values as the primary BCTZ detection parameter. Figures 5 and 6 show such data from the WAIS Divide and NEEM ice cores, respectively, in the top panels. In the WAIS Divide core the BCTZ covers the 650–1300 m depth range (corresponding to 2700 to 6000 years BP). In the NEEM ice core the BCTZ covers the depth/time range from 609 m to 1281 m (3000 to 9000 years BP).[19]

For our purposes here it is sufficient to correct the data only for gravitational firn fractionation, because the BCTZ alterations are fairly strong and because during the involved time windows (Holocene) surface temperatures/thermal fractionations were fairly constant/small.[23] For the WAIS Divide data we use $\delta^{40}Ar$ values for gravitational correction following Headly and Severinghaus[1] while for the NEEM data we use $\delta^{86}Kr$ values accordingly. The NEEM ice has experienced significant warming during storage (up to −5°C), potentially causing fractionation due to gas loss, in particular for species with a small collision diameter. In fact, if $\delta^{40}Ar$ values are used for gravitational correction in the NEEM data, the noble gas ratios in the undisturbed/shallow part (Figure 6, bottom) lie around −1‰, whereas they are expected to be around 0‰ (which is the case if $\delta^{86}Kr$ values are used). This could be explained by increased gas-loss fractionation during the warm storage period, as found by Severinghaus et al,[8] which depends on the collision diameter of the individual species, as shown by Huber et al.[24] If true this would suggest preferential loss of ^{36}Ar with respect to ^{40}Ar during this warm core handling episode, and explain why Kr isotopes (with a bigger collision diameter) are more suitable for gravitational correction in this case.

The data from the WAIS Divide core (Figure 5) are better suited to identify the effects of the BCTZ because (1) they cover a wider range around the BCTZ, (2) all data is well within the "stable" Holocene period, and (3) the ice has not suffered from warm storage (in fact, this ice has been stored with extraordinary care at cold temperature (−50°C) for most of the time). Using $\delta Ar/N_2$ values as a BCTZ indicator in this dataset, the depth range between 1120 and 1370 m (two samples marked by the gray bar) show the expected positive anomalies/excursions characteristic of the BCTZ. For these two samples, the heavy noble gas ratios show a much

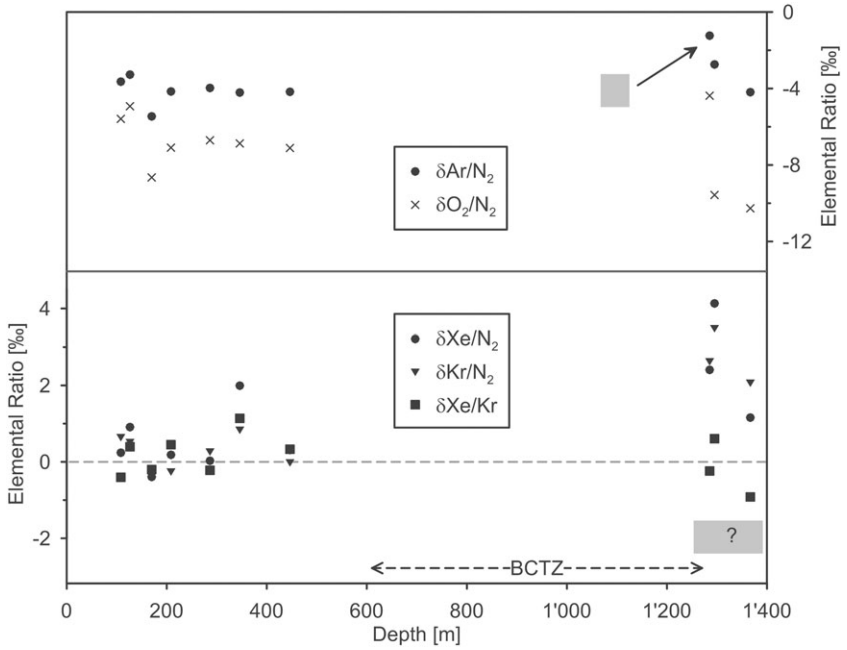

FIGURE 6 Parameters of trapped gases in ice samples from the NEEM ice core obtained with Method 1, covering roughly the last 10,000 years (Holocene). Data and graphical marks (gray bar and dashed arrow) are similar to Figure 5 while here the gravitational fractionation correction is based on measured $\delta^{86}Kr$ values instead of $\delta^{40}Ar$ values (see text for more details). Top panel: $\delta Ar/N_2$ and $\delta O_2/N_2$ with one clear positive excursion in $\delta Ar/N_2$ at 1285 m depth. Bottom panel: Noble gas elemental ratios $\delta Kr/N_2$, $\delta Xe/N_2$ and $\delta Xe/Kr$, suggesting that the BCTZ effects on these parameters (large spread) have affected all samples in the deep section (1285–1370 m). Note that the BCTZ identification made based on these data is more uncertain than for the data in Figure 5 because of the sparse data coverage and the fact that the samples also warmed significantly in the field

larger spread than that found for the first two and last three samples of the record (which should not be affected by the BCTZ). This indicates selective loss for heavy noble gases within and below the BCTZ (the "spread" is independent of the isotope ratio used for gravitational correction); however, this "spread" pattern is also seen in the two following samples below the ones identified by the $\delta Ar/N_2$ values. This suggests that the problematic depth range for noble gas ratios reaches down to 1510 m and, hence, has a longer "tail" than can be identified with the $\delta Ar/N_2$ values. The isotope ratios (Figure 5, bottom panel) show only abnormal patterns for one data point, showing that isotope ratios are not affected by the BCTZ as strongly as elemental ratios. Note that this is a fairly qualitative identification of the BCTZ and depends on the assumption of stable ocean temperatures and firn-fractionation processes over the observed period.

If the BCTZ-affected range found for the WAIS Divide ice core is also applicable for the NEEM ice core, the samples that we analyzed between 1200 and 1400 m depth in this core should also be altered by the BCTZ. The $\delta Ar/N_2$ values only show one clear positive excursion in the suspected depth range, but the heavy noble gas ratios indicate BCTZ effects in all samples of this range. Due to the sparse data from the NEEM core and the fact that this core was warmed significantly in the field, the interpretation of this data is ambiguous. As more data becomes available in the future, however, it might be possible to rule out some of the issues associated with bad ice quality and ice around the BCTZ.

Nevertheless, the data from the WAIS Divide and NEEM ice cores indicate that the heavy noble gas ratios are more sensitive to bad ice quality/BCTZ than other parameters, requiring a careful investigation of such effects, in particular if samples are taken within a few hundred meters below the conventionally determined BCTZ. Those samples not identified by positive excursions in $\delta Ar/N_2$ values but only by a spread in the noble gas ratios tend also to exhibit negative excursions in $\delta O_2/N_2$ values, suggesting that this parameter could play an important role in future outlier detection.

6 | CONCLUSIONS

The two methods that we describe here enable the determination of (heavy) noble gas elemental ratios, and their isotope ratios, in trapped air from ice samples. For the three elemental ratios $\delta Kr/N_2$, $\delta Xe/N_2$ and $\delta Xe/Kr$, which are obtained via peak jumping, precisions of 130–200, 130–310 and 110–210 per meg are reached, respectively. This is sufficient to provide a constraint on mean ocean temperatures on glacial–interglacial timescales.[1] The expected uncertainties (standard deviations) on ocean temperature reconstructions are 0.32–0.21°C for $\delta Kr/N_2$, 0.18–0.08°C for $\delta Xe/N_2$ and 0.2–0.1°C for $\delta Xe/Kr$. For the primary isotope ratios, $\delta^{15}N$, $\delta^{40}Ar$ and $\delta^{86}Kr$ values, precisions of 0.7–3.3, 3–7 and 15 per meg are reached, respectively. This allows precise reconstructions of the firn-fractionation processes[4] that have to be taken into account to reconstruct the true changes in the atmosphere.[1]

Both successively developed methods presented here allow measurement of the targeted parameters with reasonable precision; however, the latest method (Method 2) has the following advantages with respect to the earlier Method 1:

1. It can be run twice as fast (two samples per day).
2. It is less labor-intensive and therefore less prone to operator-induced artifacts and errors.
3. Several key components (water trap 2 temperature, isothermal status during splitting, equilibration time and process) are better controlled and/or investigated.
4. The precision of the $\delta^{15}N$ values is at least 30% better.
5. The precision of the $\delta Kr/N_2$, $\delta Xe/N_2$ and $\delta Xe/Kr$ values is 30% to 60% better.

In particular, the increased sample throughput is important if a larger measurement campaign is planned (with several tens to one hundred samples). The main reason for the improvements in precision is probably the more complete gas equilibration in Method 2, which was a key target

in the development of this method. Because the different heavy noble gas ratios are differently sensitive to artifacts such as (1) thermal fractionation during the processing, (2) fractionation in bad quality ice, and (3) probably also incomplete equilibration, it is suggested that all three ratios in combination are used as a proxy for ocean temperature, as they all should contain the same ocean temperature signal.[1,3]

In addition, an unexpected source of gas fractionation during the sample processing was observed called "adiabatic fractionation" (in contrast to thermal fractionation), which is new to us and might be of importance for other gas processing/analytical applications. The effect occurs when gas is compressed and expanded in a closed system. We hypothesize that the warming and cooling of the gas due to the adiabatic compression and expansion lead to local thermal fractionation in the assembly, causing the fractionation that we observe.

ACKNOWLEDGEMENTS

This work was supported by the Swiss National Science Foundation scholarship P2BEP2_152071 (to B.B.), US National Science Foundation grants 05-38630 and 09-44343 (to J.S.) and JSPS KAKENHI grants 21671001, 26241011, 15KK0027 and 17H06320 (to K.K.). We acknowledge Sarah Shackleton and Daniel Baggenstos for excellent help in the lab. Ralph Keeling pointed out the importance of adiabatic fractionation. Data used here are available on request from the corresponding author. NEEM is directed and organized by the Center for Ice and Climate at the Niels Bohr Institute and US NSF, Office of Polar Programs. It is supported by funding agencies and institutions in Belgium (FNRS-CFB and FWO), Canada (NRCan/GSC), China (CAS), Denmark (FIST), France (IPEV, CNRS/INSU, CEA and ANR), Germany (AWI), Iceland (RannIs), Japan (NIPR), Korea (KOPRI), The Netherlands (NWO/ALW), Sweden (VR), Switzerland (SNF), United Kingdom (NERC) and the USA (US NSF, Office of Polar Programs).

ORCID

Bernhard Bereiter http://orcid.org/0000-0002-1500-8617
Kenji Kawamura http://orcid.org/0000-0003-1163-700X
Jeffrey P. Severinghaus http://orcid.org/0000-0001-8883-3119

REFERENCES

1. Headly MA, Severinghaus JP. A method to measure Kr/N_2 ratios in air bubbles trapped in ice cores and its application in reconstructing past mean ocean temperature. *J Geophys Res*. 2007;112:D19105.
2. Elderfield H, Ferretti P, Greaves M, et al. Evolution of ocean temperature and ice volume through the Mid-Pleistocene climate transition. *Science*. 2012;337(6095):704-709. https://doi.org/10.1126/science.1221294
3. Ritz SP, Stocker TF, Severinghaus JP. Noble gases as proxies of mean ocean temperature: sensitivity studies using a climate model of reduced complexity. *Quat Sci Rev*. 2011;30:3728-3741.
4. Kawamura K, Severinghaus JP, Albert MR, et al. Kinetic fractionation of gases by deep air convection in polar firn. *Atmos Chem Phys*. 2013;13:11141-11155.
5. Headly MA. Krypton and xenon in air trapped in polar ice cores: Paleo-atmospheric measurements for estimating past mean ocean temperature and summer snowmelt frequency. *PhD thesis*, San Diego: University of California; 2008.
6. Buizert C, Severinghaus JP. Dispersion in deep polar firn driven by synoptic-scale surface pressure variability. *Cryosphere*. 2016;10(5):2099-2111.
7. Bereiter B, Shackleton S, Baggenstos D, Kawamura K, Severinghaus J. Mean global ocean temperatures during the last glacial transition. *Nature*. 2018;553(7686):39-44. https://doi.org/10.1038/nature25152
8. Severinghaus JP, Grachev A, Luz B, Caillon N. A method for precise measurement of argon 40/36 and krypton/argon ratios in trapped air in polar ice with applications to past firn thickness and abrupt climate change in Greenland and at Siple Dome, Antarctica. *Geochim Cosmochim Acta*. 2003;(3):325-343.
9. Severinghaus JP, Battle MO. Fractionation of gases in polar ice during bubble close-off: New constraints from firn air Ne, Kr and Xe observations. *Earth Planet Sci Lett*. 2006;244:474-500.
10. Orsi AJ. Temperature reconstruction at the West Antarctic Ice Sheet Divide for the last millennium from the combination of borehole temperature and inert gas isotope measurements. *PhD thesis*, San Diego: University of California; 2013.
11. Coplen TB. Guidelines and recommended terms for expression of stable-isotope-ratio and gas-ratio measurement results. *Rapid Commun Mass Spectrom*. 2011;25(17):2538-2560. https://doi.org/10.1002/rcm.5129
12. Martinerie P, Raynaud D, Etheridge DM, Barnola J-M, Mazaudier D. Physical and climatic parameters which influence the air content in polar ice. *Earth Planet Sci Lett*. 1992;112:1-13.
13. Bereiter B, Schwander J, Lüthi D, Stocker TF. Change in CO_2 concentration and O_2/N_2 ratio in ice cores due to molecular diffusion. *Geophys Res Lett*. 2009;36:L05703. https://doi.org/10.1029/2008GL036737
14. Petrenko VV, Severinghaus JP, Brook EJ, et al. A novel method for obtaining very large ancient air samples from ablating glacial ice for analyses of methane radiocarbon. *J Glaciol*. 2008;54(185):233-244.
15. Keeling RF, Manning AC, McEvoy EM, Shertz SR. Methods for measuring changes in atmospheric O_2 concentration and their application in southern hemisphere air. *J Geophys Res*. 1998;103(D3):3381-3397. https://doi.org/10.1029/97JD02537
16. Sarmiento JL, Gruber N. *Ocean Biogeochemical Dynamics*. Princeton University Press: Princeton; 2006.
17. Hamme RC, Emerson SR. The solubility of neon, nitrogen and argon in distilled water and seawater. *Deep Res I*. 2004;51:1517-1528.
18. Weiss RF, Kyser TK. Solubility of krypton in water and seawater. *J Chem Thermodyn*. 1978;23(1):69-72.
19. Neff P. A review of the brittle ice zone in polar ice cores. *Ann Glaciol*. 2014;55(68):72-82. https://doi.org/10.3189/2014AoG68A023
20. Kobashi T, Severinghaus JP, Kawamura K. Argon and nitrogen isotopes of trapped air in the GISP2 ice core during the Holocene epoch (0–11,500 B.P.): Methodology and implications for gas loss processes. *Geochim Cosmochim Acta*. 2008;72:4675-4686.
21. Lüthi D, Bereiter B, Stauffer B, et al. CO_2 and O_2/N_2 variations in and just below the bubble-clathrate transformation zone of Antarctic ice cores. *Earth Plant Sci Lett*. 2010;297:226-233.
22. Bereiter B, Fischer H, Schwander J, Stocker TF. Diffusive equilibration of N_2, O_2 and CO_2 mixing ratios in a 1.5-million-years-old ice core. *Cryosphere*. 2014;8(1):245-256. https://doi.org/10.5194/tc-8-245-2014
23. Cuffey KM, Clow GD, Steig EJ, et al. Deglacial temperature history of West Antarctica. *Proc Natl Acad Sci*. 2016;113:14249-14254.
24. Huber C, Beyerle U, Leuenberger M, et al. Evidence for molecular size dependent gas fractionation in firn air derived from noble gases, oxygen, and nitrogen measurements. *Earth Planet Sci Lett*. 2006;243:61-73.

How to cite this article: Bereiter B, Kawamura K, Severinghaus JP. New methods for measuring atmospheric heavy noble gas isotope and elemental ratios in ice core samples. *Rapid Commun Mass Spectrom*. 2018;32:801–814. https://doi.org/10.1002/rcm.8099